nature nanotechnology

ARTICLES

PUBLISHED ONLINE: 24 APRIL 2011 | DOI: 10.1038/NNANO.2011.58

The effect of sedimentation and diffusion on cellular uptake of gold nanoparticles

Eun Chul Cho†, Qiang Zhang and Younan Xia*

In vitro **experiments typically measure the uptake of nanoparticles by exposing cells at the bottom of a culture plate to a suspension of nanoparticles, and it is generally assumed that this suspension is well-dispersed. However, nanoparticles can sediment, which means that the concentration of nanoparticles on the cell surface may be higher than the initial bulk concentration, and this could lead to increased uptake by cells. Here, we use upright and inverted cell culture configurations to show that cellular uptake of gold nanoparticles depends on the sedimentation and diffusion velocities of the nanoparticles and is independent of size, shape, density, surface coating and initial concentration of the nanoparticles. Generally, more nanoparticles are taken up in the upright configuration than in the inverted one, and nanoparticles with faster sedimentation rates showed greater differences in uptake between the two configurations. Our results suggest that sedimentation needs to be considered when performing *in vitro* studies for large and/or heavy nanoparticles.**

Nanoparticles have been used as carriers to deliver genetic materials into cells and therapeutic agents into tumours by taking advantage of the enhanced permeation and retention (EPR) effect[1,2], and to regulate the release of drug molecules according to the physiological states of an organism[3,4]. Their superior magnetic, optical and/or photothermal properties have also been used in disease diagnosis and treatment[5–11]. In the meantime, the potential toxicity of nanoparticles has become of public concern[12–14]. All these studies of applications and toxicity rely on our ability to quantify the interactions between nanoparticles and cells, including their uptake by cells. Many reports have shown that the cellular uptake of nanoparticles depends on their size[15–19], shape[20,21] and surface coating[22–27]. Here, we demonstrate that all earlier work may need to be re-evaluated to account for the effects of sedimentation on nanoparticle dosimetry[13,14].

In a typical *in vitro* experiment, cells are immobilized at the bottom of a culture plate or on a substrate placed at the bottom of a culture plate, and incubated with a suspension of nanoparticles. The nanoparticles are assumed to be well-dispersed in the culture medium as a result of diffusion (or Brownian motion), so the concentration of nanoparticles at the cell surface is assumed to be the same as that of the initial bulk concentration. However, some nanoparticles may aggregate and change their physical characteristics when exposed to the culture medium[28]. Moreover, large and heavy nanoparticles can sediment quickly, causing the dose of nanoparticles on the cell surface to vary; in such cases, the actual concentration of nanoparticles for cellular uptake could be significantly different from the initial value. Because cellular uptake is directly related to the concentration of nanoparticles[29], the results from such studies could be inaccurate and misleading. Although a recent theoretical study has considered the effect of sedimentation and diffusion of nanoparticles on their dosimetry[30], it is important to understand how the physical parameters of nanoparticles (such as size, shape, density and surface coating) influence their transport properties (typically described as diffusion and sedimentation) in a culture medium, and how these properties affect cellular uptake. By culturing cells with gold nanoparticles in both upright and inverted configurations, we demonstrate that in the absence of particle aggregation, the cellular uptake of nanoparticles depends on the ratio of sedimentation to diffusion velocities, regardless of size, shape, density, surface coating and initial concentration.

Upright versus inverted configurations

We measured the number of gold nanoparticles taken up by cells in upright and inverted configurations (Fig. 1a) and correlated the disparity in uptake values with the sedimentation and diffusion velocities of the nanoparticles. We used a six-well culture plate, with each well containing a glass coverslip on which cells were immobilized. In the upright configuration, the coverslip containing cells was placed at the bottom of a well and incubated with a suspension of particles as is commonly done in the literature. In the inverted configuration, the coverslip was suspended from above (with the cells facing the bottom of the well) by gluing a small block of rubber on the back side of the coverslip and a syringe needle to the inner side of the cover of the culture plate. This way, we could easily position the cells in an inverted configuration immediately before an uptake experiment by inserting the syringe needle into the rubber block. The needle was cut to a length such that the cells would hang ~1.2 mm above the bottom of the well, thus minimizing any difference in liquid height above the cells in the two configurations. By using the same batch of coverslips for all experiments, we could reduce the difference in cell morphology and uptake activity caused by dissimilar surfaces[31]. The medium in each well was 5.2 mm deep, and the cells were positioned ~0.2 mm and ~1.2 mm from the bottom of the well for the upright and inverted configurations, respectively. At the particle concentrations used, all samples showed a cell viability of over 90% relative to a control sample that was not exposed to gold nanoparticles (Supplementary Fig. S1). No difference in cell viability was observed for both configurations when the cells were cultured in medium only for 24 h (Supplementary Fig. S2).

The cells in the upright configuration were expected to experience a higher concentration of nanoparticles than the initial value if the nanoparticles sedimented under the influence of gravity (when sedimentation occurs, the concentration of nanoparticles responsible for cellular uptake will be higher than the initial concentration).

Department of Biomedical Engineering, Washington University, St. Louis, Missouri 63130, USA; †Present address: Department of Chemical Engineering, Division of Chemical and Bioengineering, Hanyang University, Seoul, 133-791, Korea. *e-mail: xia@biomed.wustl.edu

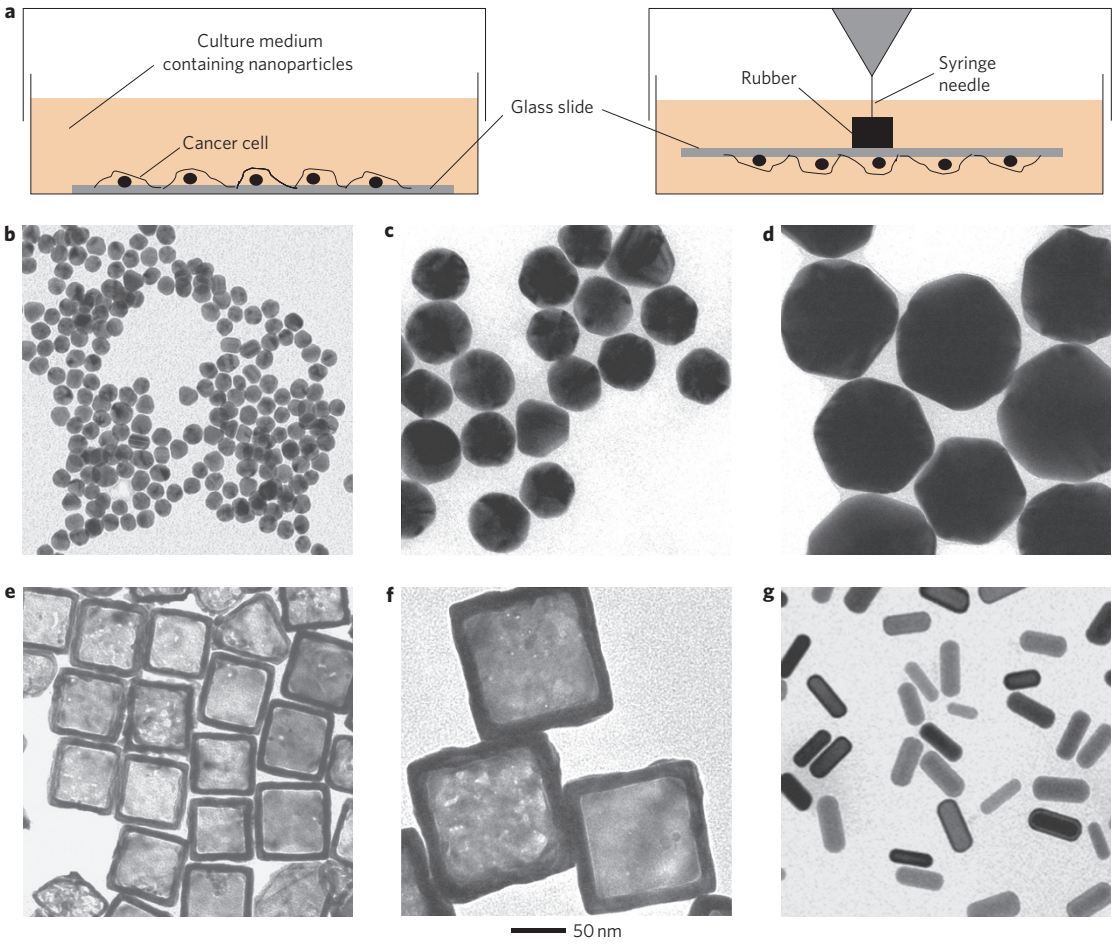

Figure 1 | Experimental setup and gold nanoparticles used in this study. a, Schematic of upright (left) and inverted (right) configurations for measuring cellular uptake of nanoparticles. Cells are not drawn to scale, and each well of a six-well culture plate contains only one glass coverslip on which cells are immobilized. **b**–**g**, TEM images showing the six types of gold nanoparticles used to examine the effects of size, shape and density on the disparity in cellular uptake between the two configurations: 15 nm (diameter) nanospheres (**b**), 54 nm nanospheres (**c**), 100 nm nanospheres (**d**), 62 nm (outer edge length) nanocages (**e**), 118 nm nanocages (**f**), nanorods (**g**, 16 nm × 40 nm, diameter by length). The 50 nm scale bar applies to all images.

Table 1 | Hydrodynamic diameters (d_h) and surface charges of gold nanoparticles before and after incubation in cell culture medium.

Gold nanoparticles		$d_{h,water}$ (nm)*				Zeta-potentials (mV)†			
		As-prepared		PEGylated		As-prepared		PEGylated	
		Before	After	Before	After	Before	After	Before	After
Nanospheres	15 nm‡	17.5	24.3	21.0	22.3	−13.7±1.1	−14.2±1.7	0.0±4.0	−9.2±3.0
	54 nm‡	55.4	84.8	67.0	75.6	−16.1±2.9	−12.7±1.7	−1.0±3.8	−9.3±1.8
	100 nm‡	96.9	133.0	108.6	124.0	−17.3±2.8	−15.1±2.1	−1.3±3.4	−12.7±3.2
Nanocages	62 nm‡	101.4	118.0	110.3	114.8	−6.6±2.8	−12.5±1.3	+0.3±3.6	−12.0±1.5
	118 nm‡	144.9	187.0	164.1	165.3	−25.5±1.8	−15.4±1.2	+1.4±2.9	−6.6±3.4
Nanorods	16 nm × 40 nm‡	23.4	29.2	24.0	26.3	+20.2±2.8	−15.9±2.0	+2.8±1.8	−12.7±0.5

See Supplementary Methods S2 and S3 for experimental details.
*The $d_{h,water}$ values were measured in deionized water. Here, 'before' and 'after' refer to samples before and after incubation in the culture medium, respectively. After incubation for 24 h, the nanoparticles were centrifuged, collected and re-dispersed in deionized water. For d_h values measured for nanoparticles dispersed in the culture medium, see Supplementary Tables S6 and S7. The difference between 'after' and 'before' corresponds to the thickness of serum proteins adsorbed from the culture medium.
†Surface charges were measured while the nanoparticles were dispersed in deionized water. The errors are standard errors ($n \geq 2$).
‡Sizes were measured from TEM images.

Conversely, cells in the inverted configuration are expected to show an opposite trend, because sedimentation will reduce the concentration of nanoparticles on the cell surface. We anticipate that the disparity in cellular uptake between the two configurations will be negligible when diffusion prevails over sedimentation, whereas the disparity will be significant when sedimentation prevails over diffusion.

We examined six different types of gold nanoparticles: nanospheres of three sizes, nanocages of two edge lengths, and nanorods (Supplementary Method S1). Figure 1b–g presents transmission electron microscopy (TEM) images of these nanoparticles. The surfaces of the nanoparticles (also termed, hereafter, 'as-prepared' samples) were covered with citrate ions (on the nanospheres), a

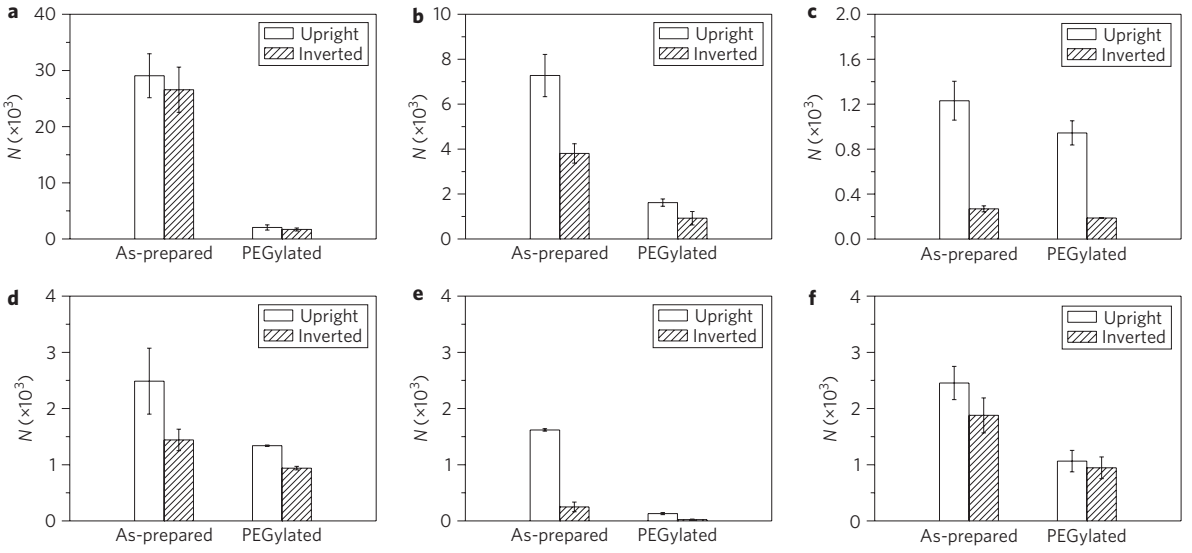

Figure 2 | Uptake values of various types of gold nanoparticles for cells positioned in upright and inverted configurations. a–f, Number (*N*) of particles taken up per cell, for both as-prepared and PEGylated samples, using the UV-vis method. The nanoparticles (and their concentrations, based on particle number) incubated with the cells: 15 nm nanospheres (**a**, 120 pM); 54 nm nanospheres (**b**, 20 pM); 100 nm nanospheres (**c**, 2.8 pM); 62 nm nanocages (**d**, 20 pM); 118 nm nanocages (**e**, 2.6 pM); and nanorods (**f**, 20 pM). Error bars are standard errors with $n = 4$.

mixture of poly(vinyl pyrrolidone) and trifluoroacetate ions (on the nanocages) and hexadecyltrimethylammonium bromide (on the nanorods). These surfaces could change following exposure to a culture medium as a result of physical and/or chemical adsorption of biomacromolecules such as serum proteins[32,33]. When serum proteins in the culture medium adsorb onto the nanoparticles, the hydrodynamic diameters of the nanoparticles increase and their surfaces became negatively charged, even though their initial surface charges measured in water typically vary from sample to sample (Table 1). The adsorbed serum proteins may induce and facilitate receptor-mediated endocytosis of the nanoparticles[32,34].

We also coated gold nanoparticles with poly(ethylene glycol) (PEG) to examine the influence of a surface coating on cellular uptake in the two configurations (Supplementary Method S1). Similar to the as-prepared samples, the surface charges of PEGylated nanoparticles changed signs when transferred to the culture medium, and this is probably owing to adsorption of serum proteins (Table 1). However, because of the antifouling properties of the PEG layer, a much smaller amount of serum protein was able to adsorb onto the PEG layer than on the as-prepared samples, and the impact of protein adsorption on cellular uptake should also be reduced[35–37].

Cellular uptake of nanoparticles

We determined the number of gold nanoparticles taken up by the cells using a UV-vis spectroscopic method[38]. According to the Beer–Lambert law, there is a linear correlation between the concentration of gold nanoparticles and the absorbance of their localized surface plasmon resonance (LSPR) peak. As such, the concentration of gold nanoparticles in a cell culture medium can be directly and quickly obtained without extensive sample preparation. We validated this method by comparing the cellular uptake data with those obtained using the conventional method based on analysis of gold content by inductively coupled plasma mass spectrometry (ICP-MS; Supplementary Tables S1 and S2). Supplementary Fig. S3 shows the UV-vis spectra of the as-prepared gold nanoparticles dispersed in a culture medium, before and after 24 h incubation with cells in the two different configurations. We used Dulbecco's modified Eagle's medium (DMEM), which is free of phenol red, because this dye has a strong absorption at 550 nm, which overlaps with the LSPR peaks of both gold nanospheres and nanorods[38]. Following incubation of the nanoparticles with the cells, the intensity of the LSPR peaks decreased. Notably, the drop was greater in the upright configuration than in the inverted configuration for the same sample of nanoparticles. We also observed a similar trend for the PEGylated nanoparticles (Supplementary Fig. S4).

Based on the UV-vis spectra, the corresponding calibration curves (Supplementary Fig. S5) and the number of cells in each sample, we calculated the number of nanoparticles taken up per cell in the two different configurations (Fig. 2). The uptake values of the as-prepared nanoparticles were much higher than those of the PEGylated nanoparticles. Furthermore, uptake was generally

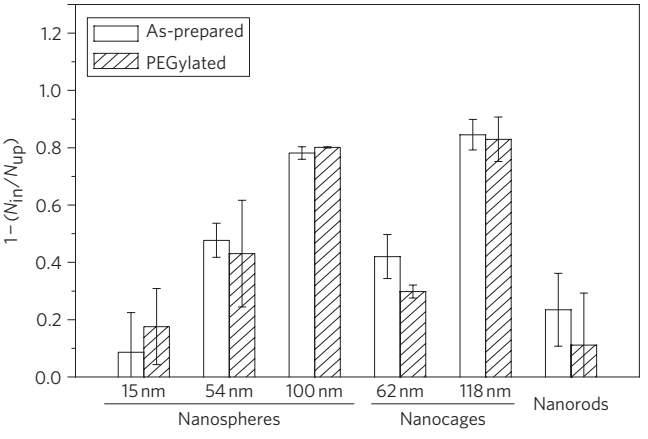

Figure 3 | Comparison of the disparity in cellular uptake between upright and inverted configurations for different types of gold nanoparticles. The disparity in uptakes between the two configurations is expressed as $1 - (N_{in}/N_{up})$, where N_{up} and N_{in} are the number of nanoparticles taken up per cell in the upright and inverted configurations, respectively. The disparity increases with particle size for both nanospheres and nanocages. Furthermore, the disparity is insensitive to surface coating for all types of nanoparticles. Error bars are standard errors with $n = 4$.

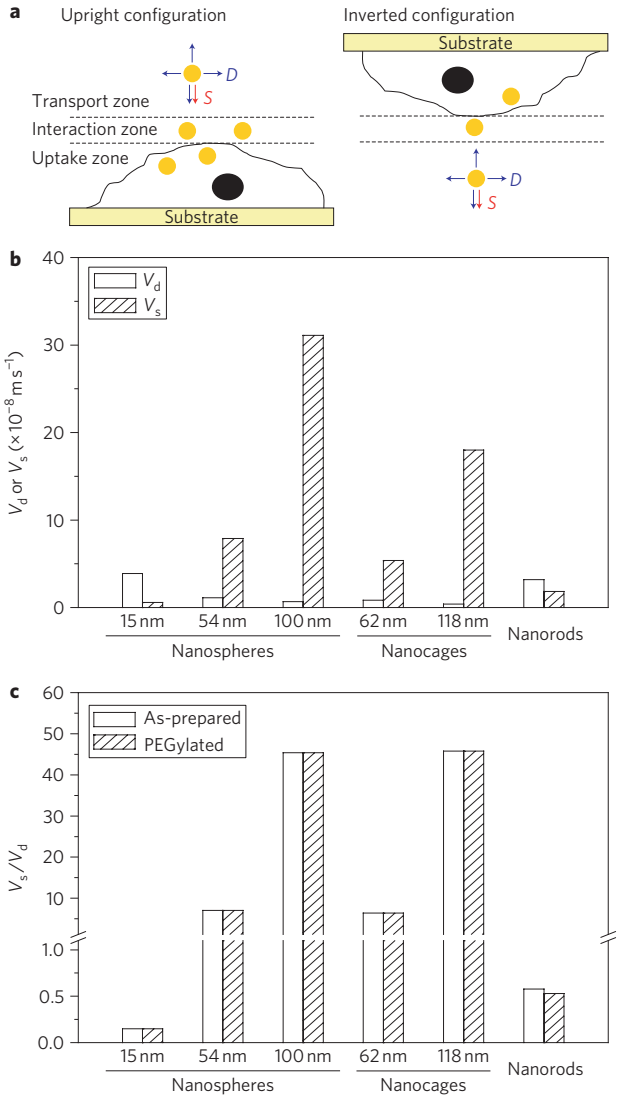

Figure 4 | Different zones involved in cellular uptake of gold nanoparticles and the two factors affecting the uptake process. a, Schematic showing transport, interaction and uptake zones when the cell is positioned in upright (left) or inverted (right) configurations. The concentration of nanoparticles in the interaction zone for both configurations may differ depending on the sedimentation (S) and diffusion (D) characteristics of the nanoparticles. **b**, Diffusion (V_d) and sedimentation (V_s) velocities of the as-prepared nanoparticles. **c**, Ratios of sedimentation and diffusion velocities (V_s/V_d) for various types of nanoparticles. The ratios determine which factor is dominant in transporting the nanoparticles to the cell surface, thereby affecting the uptake process.

higher for cells in the upright configuration than in the inverted configuration, and the disparity in cellular uptake between the two configurations was dependent on the physical parameters of the nanoparticles.

Figure 3 summarizes the disparity in cellular uptake between the two configurations for all the gold nanoparticles tested. In the plot, we express the disparity as $1 - (N_{in}/N_{up})$, where N_{up} and N_{in} are the number of nanoparticles taken up per cell in the upright and inverted configurations, respectively. It should be emphasized that the disparity in cellular uptake cannot be attributed to the change in cellular activity that might be caused by the upside-down orientation, because the uptake values of the 15 nm nanospheres were essentially the same (within experimental error) for both configurations. Similar to the 15 nm nanospheres, the nanorods also showed little disparity. Significantly, the disparity showed a strong dependence on the size of the nanoparticles; for both nanospheres and nanocages, the disparity increased as they became larger. The disparity was insensitive to surface coating for all nanoparticles tested. Furthermore, the disparity for the as-prepared 54 nm and 100 nm nanospheres did not depend on the initial concentration of the nanoparticles (Supplementary Fig. S6). Finally, the disparity was found to be dependent on incubation time, as shown by time-dependent uptake studies with the as-prepared gold nanospheres (Supplementary Table S2 and Fig. S7). In the present work, we focused only on data obtained with just one incubation time of 24 h.

To explain the disparity in cellular uptake observed for all the different types and concentrations of gold nanoparticles, we assumed that uptake proceeded through the following stages: transport of nanoparticles to the interaction zone, attachment of nanoparticles to the cell surface through adsorption, and internalization of the nanoparticles (Fig. 4a). For a specific type of nanoparticle with a particular surface coating, the adsorption and internalization steps were expected to be essentially the same, regardless of configuration, as was confirmed by the results for the 15 nm gold nanospheres. In the interaction zone, the gravitational forces (1×10^{-19} to 1×10^{-16} N) are too small (compared with those of specific and non-specific binding, 1×10^{-12} N to 1×10^{-9} N)[39–43] to have any impact on the adsorption and desorption of the nanoparticles. Therefore, the disparity in cellular uptake for the gold nanoparticles between the two configurations should be largely caused by the difference in particle concentration in the interaction zone. For cells in the upright configuration, nanoparticles can be transported into the interaction zone through diffusion and sedimentation. In contrast, for cells positioned in the inverted configuration, the nanoparticles can only be transported into the interaction zone through diffusion; sedimentation of nanoparticles in the medium below the cells will tend to reduce the concentration of nanoparticles. Although other factors such as convective forces in the culture medium induced by thermal fluctuations, liquid flow, and vibrations from the incubator motor may influence the concentration profiles of nanoparticles, they were excluded from consideration because we did not purposely apply any of these factors. The lack of difference in cellular uptake for 15 nm nanoparticles in these two configurations also suggests that these factors were far less significant than sedimentation.

To quantify the effects of diffusion and sedimentation on cellular uptake, we determined the diffusion (V_d) and sedimentation (V_s) velocities of the nanoparticles from their hydrodynamic sizes (Fig. 4b,c; Supplementary Fig. S8 and Table S4)[13,44]. The V_d and V_s values increased in the following order: 15 nm nanospheres $>$ nanorods $>$ 54 nm nanospheres $>$ 62 nm nanocages $>$ 100 nm nanospheres $>$ 118 nm nanocages for V_d; 100 nm nanospheres $>$ 118 nm nanocages $>$ 54 nm nanospheres $>$ 62 nm nanocages $>$ nanorods $>$ 15 nm nanospheres for V_s. It is worth noting that the values of V_s for the 54 nm and 100 nm nanospheres were higher than those of nanocages with equivalent sizes, although the values of V_d for these nanospheres were higher than those of the nanocages. This can be attributed to differences in elemental composition (the nanocages were made of gold–silver alloys; Supplementary Method S1), shape (spherical versus cubic), structure (solid versus hollow) and thicknesses of the surface coating (serum proteins and PEG).

Considering these transport parameters together with the cellular uptake data, it is clear that the nanoparticles (15 nm nanospheres and nanorods) with high V_d and low V_s could move quickly to the interaction zone before sedimenting, and could therefore be supplied to the cells at similar doses in both configurations, resulting in very little disparity. However, other types of nanoparticles showed greater disparity than the 15 nm nanospheres and

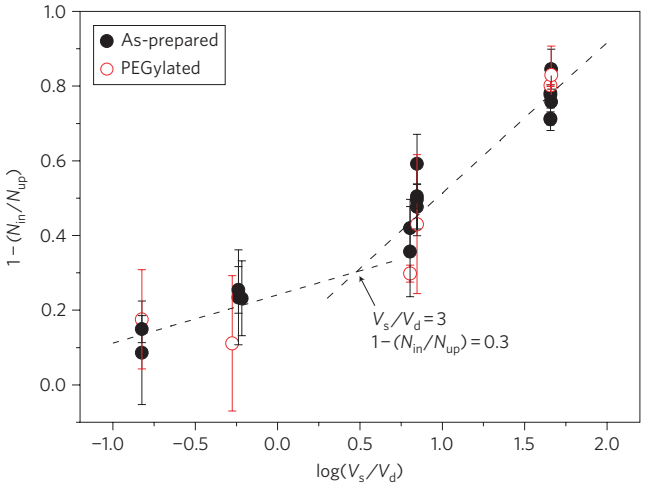

Figure 5 | Disparity in uptake between upright and inverted configurations as a function of the ratio of sedimentation and diffusion velocities. The disparity in uptake is expressed as $1-(N_{in}/N_{up})$ and the plot includes all the $1-(N_{in}/N_{up})$ values measured using both UV–vis (Fig. 3; Supplementary Figs S6 and S9) and ICP-MS methods (Supplementary Table S1). Disparity increases with increasing V_s/V_d ratio, regardless of particle size, shape, surface coating and initial concentration. The data can be grouped into two linear regions; the two dashed lines cross at $V_s/V_d = 3$, corresponding to a value of 0.3 for disparity. In general, the effect of sedimentation must be taken into consideration for nanoparticles with V_s/V_d greater than 3.

nanorods. This result implies that, in the inverted configuration, large nanoparticles (low V_d and high V_s) tend to sediment quickly before reaching the interaction zone through diffusion; more nanoparticles would therefore accumulate in the interaction zone in the upright configuration, owing to sedimentation.

To better understand the effects of V_s and V_d on the disparity in cellular uptake between these two configurations, we plotted $1-(N_{in}/N_{up})$ as a function of $\log(V_s/V_d)$ in Fig. 5. Because all the physical parameters (size, shape and density) of the nanoparticles are reflected in V_s/V_d, we could express the disparity in terms of this dimensionless ratio, regardless of the other parameters. To make the plot more general, we included $1-(N_{in}/N_{up})$ values obtained from the as-prepared 54 nm and 100 nm nanospheres at other initial concentrations (Supplementary Fig. S6) and for a different sample of as-prepared nanorods (Supplementary Fig. S9). Furthermore, we included the $1-(N_{in}/N_{up})$ values calculated using the data obtained by ICP-MS analysis of the gold content in cells (Supplementary Table S1). From this plot, one can clearly see how the disparity was affected by the composite effect of sedimentation and diffusion. In general, the disparity increased with increasing $\log(V_s/V_d)$. Somehow, the experimental data can be grouped into two linear regions with the two regression lines crossing at a value of 3 for V_s/V_d, which corresponds to a disparity of 0.3. This point lies between those for the nanorods and those for the 54 nm nanospheres (or the 62 nm nanocages), suggesting that caution must be taken when designing an experiment to study cellular uptake using gold nanoparticles with hydrodynamic diameters >40 nm, especially if one wants to determine how the size of nanoparticles affects cellular uptake.

Discussion

The model shown in Fig. 4a suggests that the disparity in cellular uptake between the two configurations was caused by the difference in particle concentration in the interaction zone resulting from sedimentation. This argument is based on the assumption that free diffusion of all components in the culture media (including the diffusion of nanoparticles) is the same in both configurations. Based on the uptake values for 15 nm nanospheres, we can conclude that the volume of the culture medium and the components in the medium to which the cells were exposed (which we call accessible volume) were more or less identical for the two configurations. If a major difference in accessible volume existed, we would expect to see a clear difference in cellular uptake for the 15 nm nanospheres in the two configurations, because such small particles should not sediment. Because the cellular uptake values were essentially the same, the cells in both configurations must be supplied with a similar dose of 15 nm nanospheres in the interaction zone. Experimentally, the separation (1.2 mm) between the cells and the bottom of the well in the inverted configuration was sufficiently wide to allow the culture medium to easily pass through without being trapped. No back flow was observed for the culture medium in the inverted configuration when we pipetted the medium. Furthermore, cell viability was almost identical for the two configurations, indicating that the separation was wide enough to allow for free bulk diffusion of all components in the culture medium.

We also compared the diffusion (V_d) and sedimentation (V_s) velocities of the nanoparticles to see if back diffusion owing to the concentration gradient was a problem (Supplementary Method S8). For the 15 nm nanospheres and nanorods, V_d was larger than V_s ($V_s/V_d < 1$), indicating that diffusion was the prevailing means for transporting nanoparticles to the cell surface, and back diffusion should not have been involved owing to the lack of a concentration gradient. For the 100 nm nanospheres and 118 nm nanocages, V_s was much higher than V_d ($V_s/V_d \gg 1$), and the concentration decayed exponentially with increasing distance from the bottom of the culture plate owing to sedimentation. In these cases, back diffusion was also not significant[45,46]. In contrast, the V_s/V_d ratios were 7.03 and 6.38 for 54 nm nanospheres and 62 nm nanocages, respectively. It is therefore necessary to include back diffusion of these nanoparticles when estimating their concentrations as a function of height. As shown in Supplementary Fig. S10, the concentration still decayed with height, even though back diffusion was involved.

When the amount of nanoparticles taken up by cells reached a level comparable to the initial concentration, the uptake itself could also alter the concentration profile of nanoparticles in the culture medium. For the 54 nm nanospheres and the 62 nm nanocages in the upright configuration, the particles depleted by cellular uptake over a period of 24 h corresponded to a concentration of 1 pM, which was much lower than the initial particle concentration of 20 pM. As such, the change in concentration induced by cellular uptake should be much smaller relative to the change induced by sedimentation. A similar argument also holds for the 100 nm nanospheres and the 112 nm nanocages.

For the inverted configuration, sedimentation of nanoparticles on the upper side of the coverslip may also influence the cellular uptake data, but the trend should be consistent with the observation and argument we make in the present work. It does not matter if the nanoparticles are deposited on the upper side of the coverslip or the bottom of the well owing to sedimentation; the end result should be the same, with a reduction in concentration of nanoparticles on the cell surface relative to the initial solution. As such, the cellular uptake would be reduced relative to the case without sedimentation.

Conclusions

We have demonstrated that the uptake of gold nanoparticles by cells is sensitive to the configurations in which the cells are positioned. Generally, nanoparticles that sediment faster demonstrated greater differences in cellular uptake between the two configurations. So far, virtually all studies on the cellular uptake of nanoparticles have been conducted with cells in the upright configuration, which may have given rise to erroneous and misleading data,

depending on the V_s/V_d ratio. Our experimental data indicate that the issue of sedimentation (or cell culture configuration) must be considered when performing studies of cellular uptake with large and/or heavy nanoparticles.

Our study also has important implications for those who conduct permeation tests with nanoparticles and biological tissues (such as skin), which are also typically carried out with the tissue placed at the bottom of a suspension of nanoparticles[47,48]. Taken together, these results are expected to improve our understanding and modelling of the interactions between nanoparticles and cells (or tissues), and thus offer a better and more efficient way to apply nanoparticles in various biomedical applications.

Methods

Methods for the preparation and surface modification of gold nanoparticles can be found in Supplementary Method S1. Human breast cancer cells (SK-BR-3, ATCC HTB-30) were cultured on coverslips (22×22 mm^2, Corning Life Sciences) in DMEM (no phenol red, Hyclone Laboratories) supplemented with 10% fetal bovine serum (FBS, ATCC) and 1% antibiotics (penicillin and streptomycin, Invitrogen). The medium was changed every other day, and the cells were incubated at 37 °C in a humidified atmosphere containing 5% CO_2. See the main text for a detailed discussion of the experimental setup.

The cells were used for uptake studies once they had reached ~90% confluence. Typically, the cells were positioned in an upright or inverted configuration and incubated with 5.0 ml of culture medium containing gold nanoparticles at 37 °C in a six-well culture plate. After 24 h, we removed the medium from each well and added 0.8 ml of pristine medium (containing no gold nanoparticles) to wash off the loosely bound nanoparticles on the cell surface. The washing procedure was repeated twice more. A UV-vis spectrophotometer (CARY50, Varian) was used to record extinction spectra of the culture medium containing nanoparticles. We first obtained the background from 300 nm to 1,100 nm with DMEM containing FBS and antibiotics. We then recorded a spectrum of the culture medium (containing FBS, antibiotics and nanoparticles) before it was used for cell culture (denoted 'before'). After incubation with cells, we recorded a spectrum of the medium that also included solutions from the three washing steps (denoted 'upright' or 'inverted' in Supplementary Figs S3 and S4). When the removed medium was mixed with the three washing solutions, the concentration of nanoparticles was reduced as a result of dilution. For this reason, we adjusted the spectrum by accounting for the total volume (2.4 ml) of the added washing solutions. In addition, from control experiments, we found that the LSPR peak intensity tended to drop with time for the as-prepared 112 nm nanocages (this sample only) in the absence of cells, probably owing to adsorption onto the surface of the culture well (for both configurations) and the upper side of the coverslip (for the inverted configuration). For this type of nanoparticle, we corrected the uptake data by taking into account the reduction caused by surface adsorption.

We calculated the number of nanoparticles taken up by the cells based on the extinction spectra (Supplementary Figs S3 and S4) and calibration curves (Supplementary Fig. S5). At the end of each experiment, we counted the number of cells in each well using a haemocytometer. The cell number was then used to calculate the uptake value of gold nanoparticles per cell. For the inverted configuration, we found that ~3% of the cells would have migrated from the glass slide to the bottom of the well during the 24 h incubation. Therefore, for this configuration, our calculation was corrected by considering the uptake of nanoparticles by cells that migrated to the bottom of the well. For the upright configuration, the number of cells migrating from the coverslip to the culture well was negligible when compared with the inverted configuration. Each data point was obtained from four parallel samples.

Received 25 October 2010; accepted 11 March 2011; published online 24 April 2011

References

1. Ghosh, P., Han, G., De, M., Kim, C. K. & Rotello, V. M. Gold nanoparticles in delivery applications. *Adv. Drug Deliv. Rev.* **60,** 1307–1315 (2008).
2. Maeda, H., Wu, J., Sawa, T., Matsumura, Y. & Hori, K. Tumor vascular permeability and the EPR effect in macromolecular therapeutics: a review. *J. Control. Rel.* **65,** 271–284 (2000).
3. Sawant, R. M. *et al.* 'SMART' drug delivery systems: double-targeted pH-responsive pharmaceutical nanocarriers. *Bioconj. Chem.* **17,** 943–949 (2006).
4. Rosler, A., Vandermeulen, G. W. M. & Klok, H-A. Advanced drug delivery devices via self-assembly of amphiphilic block copolymers. *Adv. Drug Deliv. Rev.* **53,** 95–108 (2001).
5. Jain, P. K., Huang, X., El-Sayed, I. H. & El-Sayed, M. A. Noble metals on the nanoscale: optical and photothermal properties and some applications in imaging, sensing, biology, and medicine. *Acc. Chem. Res.* **41,** 1578–1586 (2008).
6. Skrabalak, S. E. *et al.* Gold nanocages: synthesis, properties, and applications. *Acc. Chem. Res.* **41,** 1587–1595 (2008).
7. Lal, S., Clare, S. E. & Halas, N. J. Nanoshell-enabled photothermal cancer therapy: impending clinical impact. *Acc. Chem. Res.* **41,** 1842–1851 (2008).
8. Murphy, C. J. *et al.* Gold nanoparticles in biology: beyond toxicity to cellular imaging. *Acc. Chem. Res.* **41,** 1721–1730 (2008).
9. Zerda, A. D. L. *et al.* Carbon nanotubes as photoacoustic molecular imaging agents in living mice. *Nature Nanotech.* **3,** 557–562 (2008).
10. Gao, X., Cui, Y., Levenson, R. M., Chung, L. W. K. & Nie, S. *In vivo* cancer targeting and imaging with semiconductor quantum dots. *Nature Biotechnol.* **22,** 969–976 (2004).
11. Sun, C., Lee, J. S. H. & Zhang, M. Magnetic nanoparticles in MR imaging and drug delivery. *Adv. Drug Deliv. Rev.* **60,** 1252–1265 (2008).
12. Nel, A., Xia, T., Madler, L. & Li, N. Toxic potential of materials at the nanolevel. *Science* **311,** 622–627 (2006).
13. Teeguarden, J. G., Hinderliter, P. M., Orr, G., Thrall, B. D. & Pounds, J. G. Particokinetics *in vitro*: dosimetry considerations for *in vitro* nanoparticle toxicity assessments. *Toxicol. Sci.* **95,** 300–312 (2007).
14. Lison, D. *et al.* Nominal and effective dosimetry of silica nanoparticles in cytotoxicity assays. *Toxicol. Sci.* **104,** 155–162 (2008).
15. Jiang, W., Kim, B. Y. S., Rutka, J. T. & Chan, W. C. W. Nanoparticle-mediated cellular response is size-dependent. *Nature Nanotech.* **3,** 145–150 (2008).
16. Alivisatos, A. P., Gu, W. & Larabell, C. Quantum dots as cellular probes. *Annu. Rev. Biomed. Eng.* **7,** 55–76 (2005).
17. Rejman, J., Oberle, V., Zuhorn, I. S. & Hoekstra, D. Size-dependent internalization of particles via the pathways of clathrinand caveolae-mediated endocytosis. *Biochem. J.* **377,** 159–169 (2004).
18. Panyam, J. & Labhasetwar, V. Biodegradable nanoparticles for drug and gene delivery to cells and tissue. *Adv. Drug Deliv. Rev.* **55,** 329–347 (2003).
19. Prabha, S., Zhou, W-Z., Panyam, J. & Labhasetwar, V. Size-dependency of nanoparticle-mediated gene transfection: studies with fractionated nanoparticles. *Int. J. Pharm.* **244,** 105–115 (2002).
20. Cho, E. C., Au, L., Zhang, Q. & Xia, Y. The effects of size, shape, and surface functional group old nanoparticles on their adsorption and internalization by cells. *Small* **6,** 517–522 (2010).
21. Chithrani, B. D. & Chan, W. C. W. Elucidating the mechanism of cellular uptake and removal of protein-coated gold nanoparticles of different sizes and shapes. *Nano Lett.* **7,** 1542–1550 (2007).
22. Verma, A. & Stellacci, F. Effect of surface properties on nanoparticle–cell interactions. *Small* **6,** 12–21 (2010).
23. Verma, A. *et al.* Surface-structure-regulated cell-membrane penetration by monolayer-protected nanoparticles. *Nature Mater.* **7,** 588–595 (2008).
24. Leroueil, P. R. *et al.* Nanoparticle interaction with biological membranes: does nanotechnology present a Janus face? *Acc. Chem. Res.* **40,** 335–342 (2007).
25. Cho, E. C., Xie, J., Wurm, P. A. & Xia, Y. Understanding the role of surface charges in cellular adsorption versus internalization by selectively removing gold nanoparticles on the cell surface with a I_2/KI etchant. *Nano Lett.* **9,** 1080–1084 (2009).
26. Zorko, M. & Langel, U. Cell-penetrating peptides: mechanism and kinetics of cargo delivery. *Adv. Drug Deliv. Rev.* **57,** 529–545 (2005).
27. Sudimack, J. & Lee, R. J. Targeted drug delivery via the folate receptor. *Adv. Drug Deliv. Rev.* **41,** 147–162 (2000).
28. Sager, T. M. *et al.* Improved method to disperse nanoparticles for *in vitro* and *in vivo* investigation of toxicity. *Nanotoxicology* **1,** 118–129 (2007).
29. Xu, C., Tung, G. A. & Sun, S. Size and concentration effect of gold nanoparticles on X-ray attenuation as measured on computed tomography. *Chem. Mater.* **20,** 4167–4169 (2008).
30. Hinderliter, P. M. *et al.* ISDD: a computational model of particle sedimentation, diffusion and target cell dosimetry for in vitro toxicity studies. *Particle Fibre Toxicol.* **7,** 36–54 (2010).
31. Kong, H. J. *et al.* Non-viral gene delivery regulated by stiffness of cell adhesion substrates. *Nature Mater.* **4,** 460–464 (2005).
32. Alkilany, A. M. *et al.* Cellular uptake and cytotoxicity of gold nanorods: molecular origin of cytotoxicity and surface effects. *Small* **5,** 701–708 (2009).
33. Lynch, I. *et al.* The nanoparticle–protein complex as a biological entity: a complex fluids and surface science challenge for the 21st century. *Adv. Colloid Interface Sci.* **134–135,** 167–174 (2007).
34. Conner, S. D. & Schmid, S. L. Regulated portals of entry into the cell. *Nature* **422,** 37–44 (2003).
35. Feldman, K., Ha1hner, G., Spencer, N. D., Harder, P. & Grunze, M. Probing resistance to protein adsorption of oligo(ethylene glycol)-terminated self-assembled monolayers by scanning force microscopy. *J. Am. Chem. Soc.* **121,** 10134–10141 (1999).
36. Sigal, G. B., Mrksich, M. & Whitesides, G. M. Effect of surface wettability on the adsorption of proteins and detergents. *J. Am. Chem. Soc.* **120,** 3464–3473 (1998).
37. Horbett, T. A. & Brash, J. L. (eds) *Proteins at Interfaces II* 396 (American Chemical Society, 1995).

38. Cho, E. C., Liu, Y. & Xia, Y. A simple spectroscopic method for differentiating cellular uptakes of gold nanospheres and nanorods from their mixtures. *Angew. Chem. Int. Ed.* **49,** 1976–1980 (2010).
39. Leckband, D. Nanomechanics of adhesion proteins. *Curr. Opin. Struct. Biol.* **14,** 524–530 (2004).
40. Dammer, U. *et al.* Specific antigen/antibody interactions measured by force microscopy. *Biophy. J.* **70,** 2437–2441 (1996).
41. Allen, S. *et al.* Detection of antigen–antibody binding events with the atomic force microscope. *Biochemistry* **36,** 7457–7463 (1997).
42. Tha, S. P., Shuster, J. & Goldsmith, H. L. Interaction forces between red cells agglutinated by antibody. II. Measurement of hydrodynamic force of breakup. *Biophys. J.* **50,** 1117–1126 (1986).
43. Vasir, J. K. & Labhasetwar, V. Quantification of the force of nanoparticle–cell membrane interactions and its influence on intracellular trafficking of nanoparticles. *Biomaterials* **29,** 4244–4252 (2008).
44. Hiemenz, P. C. & Rajagopalan, R. *Principles of Colloid and Surface Chemistry* 94 (Marcel Dekker, 1997).
45. Brown, P. H. & Schuck, P. Macromolecular size-and-shape distributions by sedimentation velocity analytical ultracentrifugation. *Biophys. J.* **90,** 4651–4661 (2006).
46. Sperling, R. A. *et al.* Size determination of (bio)conjugated water-soluble colloidal nanoparticles: a comparison of different techniques. *J. Phys. Chem.* **111,** 11552–11559 (2007).
47. Shim, J. *et. al.* Transdermal delivery of mixnoxidil with block copolymer nanoparticles. *J. Control. Rel.* **97,** 477–484 (2004).
48. Sonavane, G. *et al. In vitro* permeation of gold nanoparticles through rat skin and rat intestine: effect of particle size. *Colloids Sur. B* **65,** 1–10 (2008).

Acknowledgements

Y.X. thanks the National Institutes of Health (NIH) for a 2006 Director's Pioneer Award (DP1 OD000798) and a grant (1R01 CA138527). E.C.C. was also partially supported by a fellowship from the Korea Research Foundation (KRF-2007-357-D00070). Part of the work was performed at the Nano Research Facility, a member of the National Nanotechnology Infrastructure Network (NNIN), supported by the National Science Foundation (NSF) under award ECS-0335765.

Author contributions

E.C.C. and Y.X. conceived and designed the experiments. E.C.C. performed the experiments, analysed the data and prepared the manuscript. Y.X. revised the manuscript. Q.Z. synthesized the nanocages.

Additional information

The authors declare no competing financial interests. Supplementary information accompanies this paper at www.nature.com/naturenanotechnology. Reprints and permission information is available online at http://www.nature.com/reprints/. Correspondence and requests for materials should be addressed to Y.X.